23 May 2001

A Lagrangian Description of Flows in Stirred Tanks Via Computer-Automated Radioactive Particle Tracking (CARPT)

A. R. Rammohan

A. Kemoun

M. (Muthanna) H. Al-Dahhan
Missouri University of Science and Technology, aldahhanm@mst.edu

M. P. Dudukovic

Recommended Citation

A. R. Rammohan et al., "A Lagrangian Description of Flows in Stirred Tanks Via Computer-Automated Radioactive Particle Tracking (CARPT)," *Chemical Engineering Science*, vol. 56, no. 8, pp. 2629 - 2639, Elsevier, May 2001.
The definitive version is available at https://doi.org/10.1016/S0009-2509(00)00537-6

PERGAMON

Chemical Engineering Science 56 (2001) 2629–2639

Chemical Engineering Science

www.elsevier.nl/locate/ces

A Lagrangian description of flows in stirred tanks via computer-automated radioactive particle tracking (CARPT)

A. R. Rammohan, A. Kemoun, M. H. Al-Dahhan, M. P. Dudukovic*

Chemical Reaction Engineering Laboratory (CREL), Department of Chemical Engineering, Washington University, One Brookings Drive, Campus Box 1198, St. Louis, MO 63130-4899, USA

Received 25 July 2000; received in revised form 9 November 2000; accepted 9 November 2000

Abstract

In this study, computer-automated radioactive particle tracking (CARPT) is implemented for the first time in the characterization of flows in stirred tanks. Both the experimental technique and the experimental set-up are discussed. The CARPT technique is seen to capture qualitatively most of the important flow phenomena observed in stirred tank flows, like the two recirculating loops above and below the impeller and the dead zones at the bottom of the tank. The CARPT data is also used to extract "Sojourn" time distributions in different zones of the reactor. These distributions are used to partially quantify the observed dead and active zones in the tank.

Keywords: Hydrodynamics; Mixing; Multiphase flow; Visualization; Particle tracking; Non-invasive technique

1. Introduction

Stirred tank reactors (STR) are widely used in the manufacture of fine chemicals, pharmaceuticals and in paper and pulp, polymer and food industry. Most of these operations involve mixing of two or more phases. The design of stirred tanks requires the knowledge of the flow field (like velocity, turbulence intensity, holdup distribution of the dispersed phase, etc.) and the understanding of the effects of various system parameters, like impeller-type, power input, numbers of baffles, etc., on mixing efficiency. Detailed experimental data characterizing single-phase flows in stirred tanks exists in the literature (Van't Reit & Smith, 1975; Yianneskis, Popilek, & Whitelaw, 1987; Wu & Patterson, 1989; Ranade & Joshi, 1990; Yianneskis & Whitelaw, 1993; Stoots & Calabrese, 1995; Zhou & Kresta, 1996; Kemoun, Lusseyran, Mallet, & Mahoust, 1998; Schaefer & Hofken, 1999). This data has been collected using existing popular measurement techniques such as laser doppler anemometry (LDA), digital particle imaging velocimetry (DPIV), etc., all of which provide Eulerian data only that must then be related to mixing times and mixing efficiency (Wittmer, Falk, Pitiot, & Vivier, 1998). For multiphase flows, which are of considerable interest, "optical" techniques like LDA, DPIV, etc., are limited to low-volume fractions of the dispersed phase (Rousar & Van den Akker, 1994; Morud & Hjertager, 1996; Deen & Hjertager, 1999) and cannot be used to discern any information regarding the phase holdup distributions.

In contrast, computer-automated radioactive particle tracking (CARPT) and computed tomography (CT) are powerful non-invasive monitoring techniques capable of providing information in "opaque" multiphase flows that have not been employed in stirred tanks so far. CARPT and CT have been used extensively and successfully to characterize multiphase flows at high-volume fractions in a variety of multiphase reactors such as bubble columns, liquid–solid risers, etc (Chaouki, Larachi, & Dudukovic, 1997; Kumar & Dudukovic, 1997; Devanathan, Moslemian, & Dudukovic, 1990; Degaleesan & Dudukovic, 1995; Roy, Chen, Kumar, Al-Dahhan, & Dudukovic, 1997). CARPT provides the actual trajectories of a tracer particle and can be readily used in both single-phase and multi-phase systems. It yields Lagrangian information about the velocity vector along the particle trajectory from which the complete three-dimensional velocity distributions, turbulence parameters and dispersion coefficients can be obtained. Such information can be used to

* Corresponding author. Tel.: +1-314-935-6021; fax: +1-314-935-4832.

E-mail address: dudu@poly1.che.wustl.edu (M. P. Dudukovic).

0009-2509/01/$ - see front matter
PII: S0009-2509(00)00537-6

validate computational fluid dynamic (CFD) simulations in a STR. It also provides visualization and insight into the complex swirling flows in STRs. In this work, the implementation of CARPT in STRs is described. A qualitative assessment of the CARPT results obtained in a STR using water as the fluid is provided. The objective of this study is to establish the type of information that CARPT can provide in single-phase flows in stirred tanks. This is to be followed by quantitative comparison with data obtained by established techniques like LDA and DPIV. The ultimate objective is to use CARPT in opaque multiphase flows in stirred tanks at conditions inaccessible to other measurement techniques.

2. Experimental set-up

2.1. The stirred vessel

The stirred vessel used is of the standard Holland and Chapman-type (1966) consisting of a cylindrical tank with four baffles and a stirrer (Fig. 1). All the parts are made of a transparent material (clear plexiglass). The diameter of the vessel is $D = 0.2$ m. The baffles are $D/10$ in width and $D/125$ in thickness, vertical and flush with the wall. The agitator is a Rushton turbine composed of a disc of $D_I = D/3$ overall diameter with six rectangular radial blades of $w = D/15$ height and thickness $D/125$. The turbine is located at a distance D_I from the bottom of the tank which is filled with water to a height equal to the tank diameter. The shaft diameter is $D/31.5$ and the disc thickness is $D/67$.

2.2. The CARPT setup

The CARPT setup consists of 16 scintillation detectors (Fig. 2) mounted on aluminum supports, which are arranged on an octagonal base. There are eight aluminum supports placed around the tank at 45° to each other. Each support has two holes of diameter 2.2″ (5.6 cm). The axial location of the center of the holes from the octagonal base plate is as follows: The lowest hole is at a distance of $Z_1 = 2.86$ cm, then $Z_2 = 7.72$ cm, $Z_3 = 12.59$ cm and $Z_4 = 17.45$ cm. Every aluminum support has the holes placed, either at Z_1 and Z_4 or at Z_2 and Z_3. Every consecutive support has alternate locations of the holes. This configuration optimizes the extent to which the particle can be seen by each detector in the tank (Degaleesan, 1997). Each detector unit is a cylinder 2.125″ (5.4 cm) in diameter and 10.25″ (26.0 cm) long, and contains an active cylindrical sodium iodide crystal (2″ × 2″, i.e., 5.08 cm × 5.08 cm). Every axial level has four detectors each at right angles with the others. These detectors are placed at the above-mentioned four different axial levels. The detectors at each axial level are staggered by 45° with respect to the previous level. The radioactive particle (Fig. 3), the position of which is tracked, is about 2.3 mm in diameter, made of polypropylene with radioactive Scandium embedded in it (^{46}Sc, 80 μCi) and with an air pocket so that the effective density of the particle is equal to that of water (or the fluid tracked). In spite of the fact that the tracer particle is neutrally buoyant, its size is too large to enable it to follow all the energy containing eddies in the flow. This particle was chosen because it was readily available to test the CARPT technique in stirred tanks. Once feasibility is established, one can search for a more suitable tracer size while compromising between size and density mismatch. We discuss the limitations of the current tracer particle in the subsequent section.

2.3. The CARPT technique

Devanathan (1991) adapted the CARPT technique to study the motion of the liquid phase in bubble columns. A single radioactive particle that is neutrally buoyant

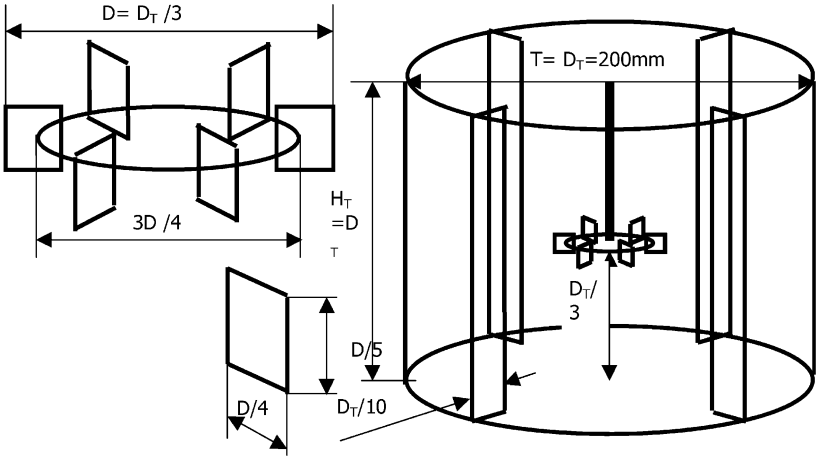

Fig. 1. Stirred tank of the Holland–Chapman-type used for the CARPT experimental study.

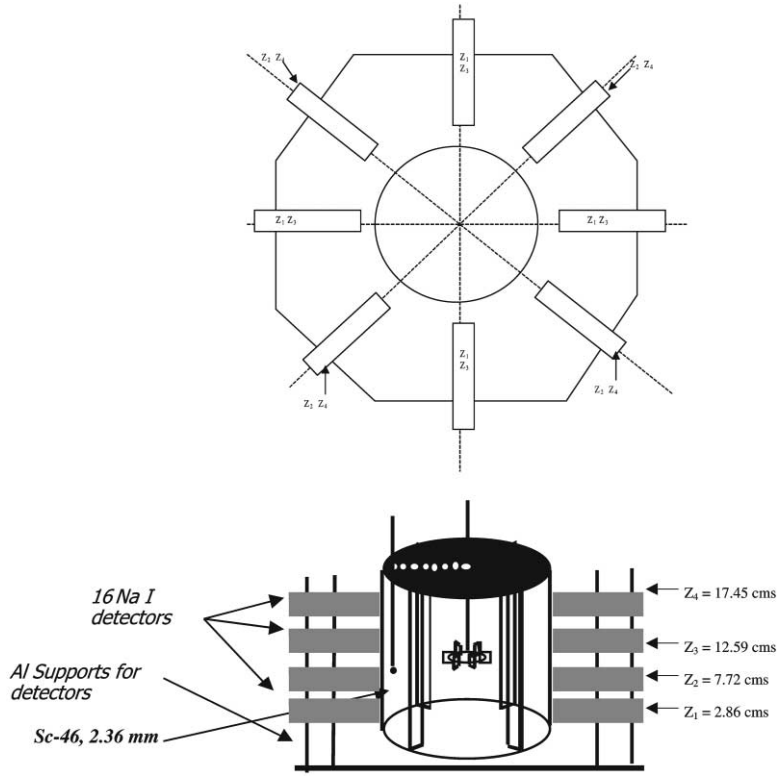

Fig. 2. CARPT setup for the stirred tank.

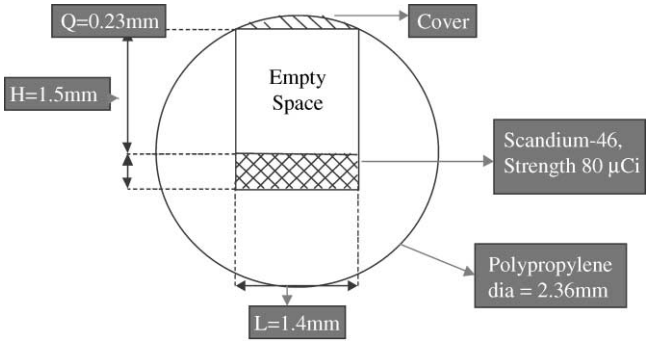

Fig. 3. Details of the CARPT tracer particle.

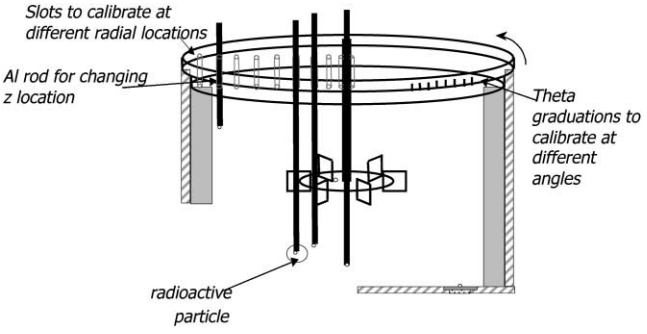

Fig. 4. Details of the calibration procedure.

with respect to the liquid being tracked was used with radioactive scandium, ^{46}Sc, emitting γ radiation employed as the isotope. During an experiment, as the particle moves about in the vessel tracking the liquid phase, the position of the particle is determined by an array of scintillation detectors that monitor the γ radiation emitted by the particle. The radiation intensity recorded at each detector decreases exponentially with increasing distance between the particle and the detector. In order to estimate the position of the particle from the radiation intensities, calibration is performed prior to a CARPT experiment by placing the particle at various known locations and monitoring the radiation recorded by each detector (Fig. 4). Using the information acquired, calibration curves are established that relate the intensity received at a detector to the distance between the particle and the detector (Fig. 5). Once the distance of the particle from the set of detectors is evaluated, a weighted regression scheme is used to estimate the position of the particle at a given sampling instant in time. Thereby a sequence of instantaneous position data is obtained that yields the position of the particle at successive sampling instants (Fig. 6). In our experiments the sampling frequency was 50 Hz, i.e., particle position is identified at 0.02 s intervals. Time differentiation of the successive particle positions yields the instantaneous Lagrangian velocities of the particle, i.e., velocities as a function of time and position of the particle. From the Lagrangian

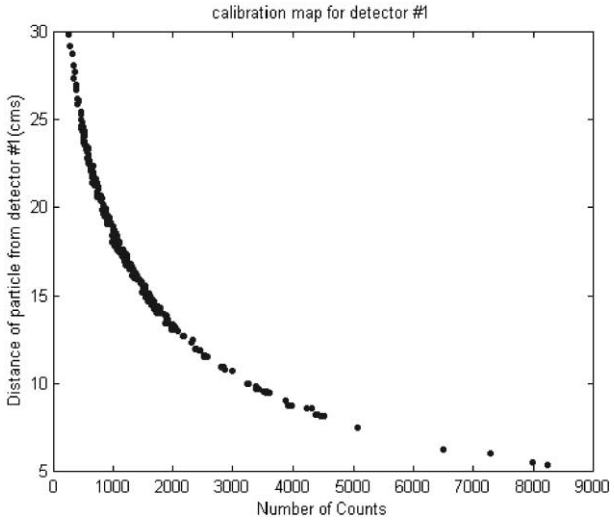

Fig. 5. Calibration map for detector #1.

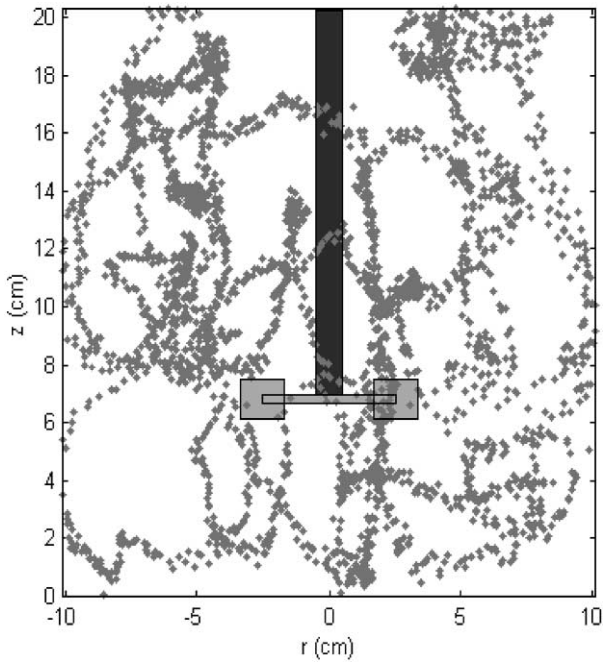

Fig. 6 . Projection of the particle trajectory in a vertical plane at $N = 150$ rpm for 30 s.

particle velocities, ensemble averaging is performed to calculate the average velocities and thereafter the various "turbulence" parameters of the liquid. Clearly, due to finite size of the particle we are not capturing the true and fine-scale liquid turbulence but rather various cross correlations of particle velocity fluctuations around the mean.

2.4. Measurement errors

2.4.1. Tracer ability to follow the liquid

The accuracy of determining the liquid velocity using the particle tracking technique depends in part on the ability of the tracer particle to follow the liquid. Close matching of the density of the particle with that of the liquid ensures that the particle is neutrally buoyant. However, the finite size of the particle makes it differ from a liquid element, unable to sample the small scale eddies. Devanathan (1991) showed that for a particle of size 2.36 mm, and a difference of 0.01 g/cm^3 in density between the particle and the liquid, the maximum difference in the velocities (between particle and liquid) is 1 cm/s. Degaleesan (1997) estimated that the maximum frequency at which the 2.36 mm particle can be taken to follow up to 99.0% of the liquid velocity is 30 Hz. She also showed that for frequencies smaller than 30 Hz, which represent the large-scale eddies, the particle will be able to closely follow the liquid phase, and the measured particle fluctuating velocities can be considered to be those of the liquid phase. Higher-frequency eddies cannot be followed by the current particle.

2.4.2. Statistical nature of gamma photons

The emission of gamma photons from a radioactive source follows a Poisson distribution (Tsoulfanidis, 1983). Therefore, every mean count reported in the calibration curve is associated with a distribution of counts. When reconstructing the particle position from the instantaneous counts registered by each detector only the mean values are used, while in reality the counts measured will be but one value from the distribution seen around the mean. Hence, the reconstructed particle position will not be the exact instantaneous position. The error in reconstructing the particle position along a known trajectory (a circular one when particle is placed in the impeller disc at $r = 6.0$ cm, $Z = 6.67$ cm) is found to be less than 3 mm.

2.4.3. Solid angle effect

Devanathan (1991) showed that the solid angle has a significant effect on the detected radiation intensity and that the side face of the detector composed of sodium iodide (NaI) cylindrical crystal is more effective than the front face from the standpoint of detection. If many detectors see the particle, each with a different solid angle, then the errors introduced by some detectors are partially compensated for by the other detectors resulting in better accuracy. To obtain higher accuracy in tracer location, solid angle effects have to be considered in the calibration. To some extent this has been implemented by Degaleesan (1997), by using a two-step method in reconstructing the particle position. In the second step, solid angle affects are taken into account. Further improvements can be accomplished by modeling the various interactions of the radiation with the medium and the detector crystal. Modeling of the gamma-ray interactions using Monte Carlo simulations has been successfully performed

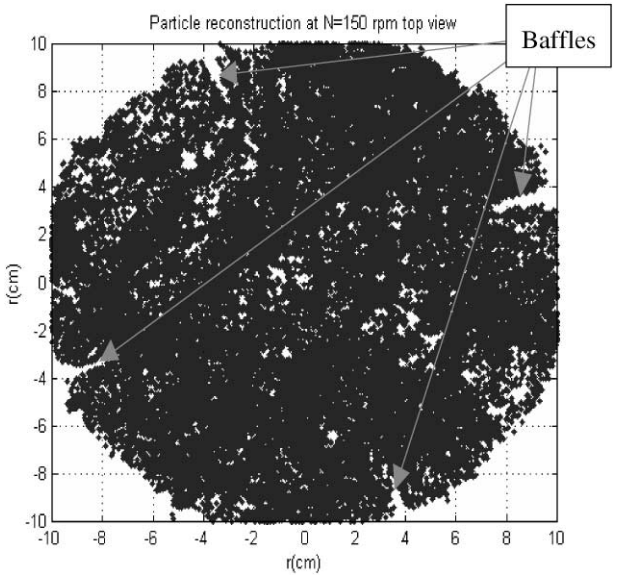

Fig. 7. Projection of the reconstructed particle position at $N = 150$ rpm, top view for 1 h of the 16 h run.

by Larachi, Kennedy, and Chaouki (1994) who has used radioactive particle tracking to study the behavior of solids in ebullated beds.

Given the above possible sources of errors in reconstructing the particle position in a stirred tank, we find the accuracy in reconstructing particle position to be reasonably good. This can be seen from the fact that the reconstructed particle positions are hardly ever located in the region of the baffles which are about 1.5 mm thick (Fig. 7).

2.5. Experimental conditions

Water is used as the fluid whose motion is tracked by the radioactive particle. Experiments were conducted at 150 rpm ($Re_{imp} = 12{,}345$) at room temperature. The height of the liquid in the tank was 20.0 cm (equal to tank diameter).

3. Results and discussion

3.1. Validity of experimental data

As a first step in establishing the validity of their experimental data, different researchers have reported mass balance verifications. The balance is usually verified in a control volume containing the impeller. These results have been summarized in Table 1. It can be seen that mass balances are usually satisfied within 1–10% accuracy. Table 1 suggests that CARPTs accuracy in closing the mass balance within 7% is comparable to other techniques.

3.2. Location of the eye of the recirculating loops

The azimuthally averaged velocity in the r–z plane is displayed in Fig. 8. The velocity vector plot captures the key qualitative features expected in this stirred tank configuration (Van der Molen & van Maanen, 1978; Yianneskis et al., 1987; Costes & Couderc, 1988a, b; Wu & Patterson, 1989; Ranade & Joshi, 1990). There is a radial jet in the plane of the impellers, which goes right to the walls. This high-speed radial jet entrains the surrounding fluid and slows down as it approaches the tank wall. Near the tank wall, the jet stream splits into two portions, one of which then circulates through the upper and the other through the lower portion of the tank and both are finally drawn back into the impeller region. These two streams result in the two recirculation loops seen in Fig. 8. One loop is above the impeller and the other below the impeller. Both circulation loops exhibit what is conventionally called the eye of the loop. The vertical position of the eye of the upper loop is found to be around $D/2$ and the eye of the bottom loop is at an elevation around $D/5$ (where D is tank diameter) with the radial location of both loops at $2D/5$. This compares well with the dimensionless locations reported by other researchers as evident from Table 2.

3.3. Mapping the dead zones in the stirred tank

At the bottom of the stirred tank, the influence of the impeller is not as pronounced as in the rest of the tank.

Table 1
Accuracy of mass balance closure

Researcher	Technique used	Region considered	Accuracy
Gunkel and Weber (1975)	HFA	$40 < z/D < 0.16, 0 < r/D < 1$	Within 4%
Yianneskis et al. (1987)	LDA	CV around impeller	Within 1%
Wu and Patterson (1989)	LDA	$-0.22 < z/D < 0.22, 0 < r/D < 0.55$	Within 1%
Ranade and Joshi (1990)	LDA	CV around impeller	Within 5%
Yianneskis and Whitelaw (1993)	LDA	CV around impeller	Within 1%
Zhou and Kresta (1996)	LDA	$-0.15 < z/D < 0.23, 0 < r/D < 0.525$	Within 5–10%
This work	CARPT	CV around the impeller	Within 7%

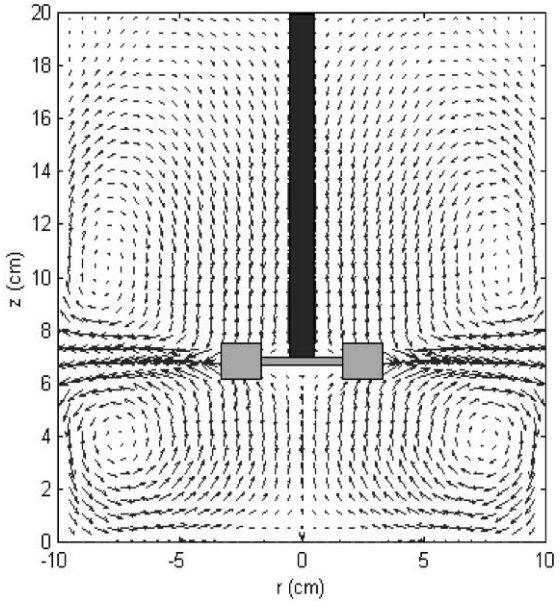

Fig. 8. Azimuthally averaged velocity vector plot at $N = 150$ rpm.

This results in regions of very low velocities at the bottom of the tank where fluid elements (or dispersed phase like solid particles) tend to spend larger time than in other portions of the tank. The presence of such regions can lower the mixing efficiency. The existence of such zones has been identified by flow visualization studies (Kemoun, 1995). Kemoun introduced a number of polypropylene beads (of $d_P = 0.3$ mm and $\rho_P = 0.8$ g/cm^3) into the water flow in the same tank configuration as used in this work and illuminated the bottom of the tank with a laser sheet. The regions with higher number of particles reflect more light and appear as the bright regions in the photograph. We reproduce here one such snapshot taken by Kemoun (1995) in Fig. 9a where the bright spots can be seen to be in the form of a starfish-like pattern. These bright regions correspond to the dead zones where particle velocities are low causing more particles to accumulate and settle. A similar plot has been generated from the CARPT data where the vector plot of the resultant of the radial and the tangential velocity at the bottom of the tank is shown in Fig. 9b. The plot is colored with the contours of the total velocity vector in this plane. The blue regions show the regions of very low velocity. The yellow regions show the regions of high velocity. At the bottom, the dead zone can be seen clearly and it seems to resemble a starfish. The interesting thing is that these dead zones seem to be due to a swirling tornado-like structure, which starts just below the impeller plane and is entirely three dimensional in nature. The instability seems to begin at the baffles and slowly propagates downward until the starfish-like pattern is observed at the bottom. This comparison of CARPT obtained results with direct flow visualisation illustrates CARPTs potential for capturing important flow phenomena.

3.4. *Partial quantification of dead zones using sojourn time distributions* (*STDs*)

In this study, we extract the sojourn time distribution (STD), i.e., strictly speaking the probability density function of sojourn times for different regions in the tank, from the CARPT experiment. For illustrative purposes we have divided the tank only in the axial (vertical) direction into ten regions, each 2 cm in height. For each of these zones we compute the STD, as illustrated below, and we display the STDs in Fig. 10. It is important to note that any desired additional compartmentalization in the angular (θ) and radial (r) direction is possible. Thus, STDs can be calculated from the experimental CARPT data for any region of interest in the stirred tank. We obtain the STD for an axial slice of the tank, defined above, as follows. From the CARPT experiment the record of the particle trajectory as a function of time is available with the time starting at zero and with every subsequent particle location recorded at intervals of $\Delta t = 0.02$ s (corresponding to $f_{\text{sample}} = 50$ Hz). Hence, the Nth particle position corresponds to the time of $N\Delta t$ seconds since the start of the experiment. To generate the STD curve for each zone, the records of the particle positions are scanned until the particle is found in the zone of interest (i.e., the axial co-ordinate of the tracer is between Z_{lower} and Z_{upper} of that zone). Now, the particle position is tracked until the tracer leaves the zone of interest. The number of consecutive occurences (say N) from the time the tracer particle entered the zone until

Table 2
Location of the eye of circulation loops ($T = D$ = tank diameter)

Researcher	Lower r/T	Lower z/T	Upper r/T	Upper z/T	Clearance H_c/T
Yianneskis et al. (1987)	0.3	0.20	0.30	0.48	0.33
Costes and Couderc (1988a, b)	0.4	0.25	0.4	0.75	0.50
Schaeffer, Hofken, and Durst (1997)	0.4	0.20	0.4	0.5	0.33
Kemoun et al. (1998)	0.4	0.20	0.4	0.5	0.33
Current work	0.4	0.20	0.4	0.5	0.33

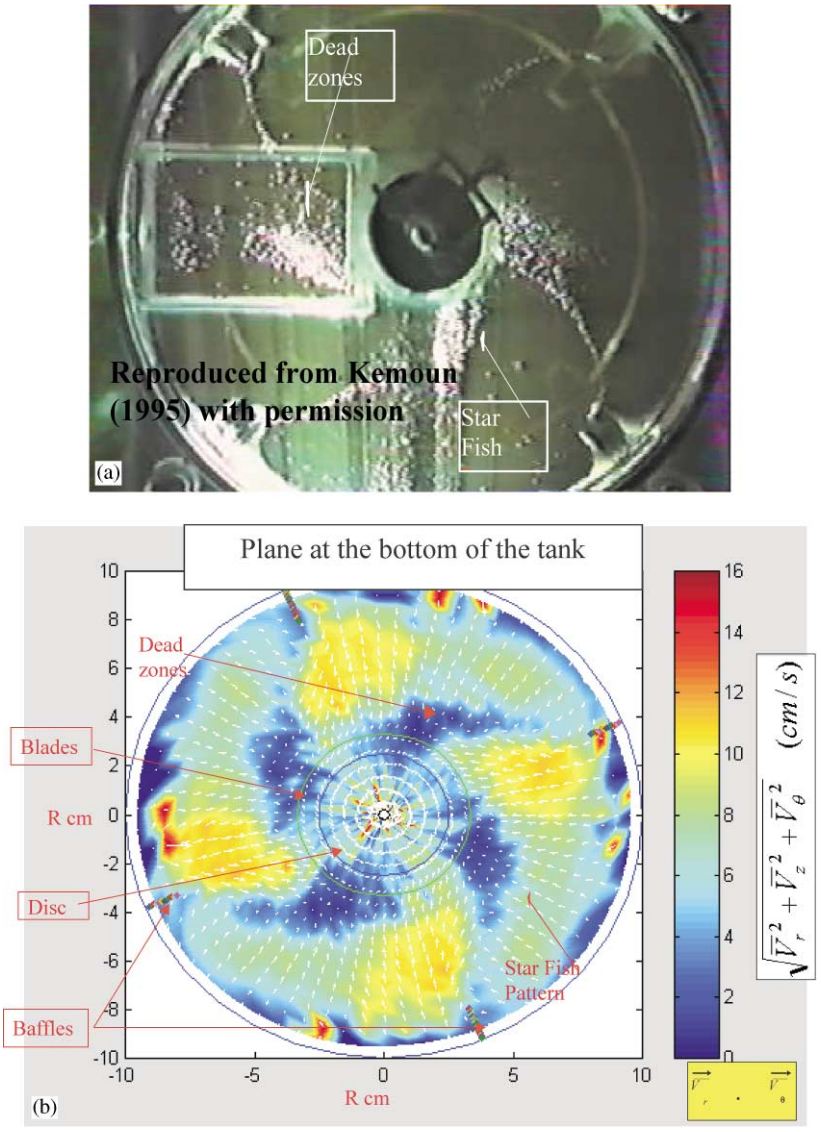

Fig. 9. (a) Dead zones from flow visualization studies (Kemoun, 1995). (b) Map of dead zones from CARPT.

the time the tracer particle leaves the zone of interest is noted. From this the sojourn time of the tracer particle during that pass through the zone of interest can be calculated as

$$t_{\mathrm{res1}} = N\Delta t. \tag{1}$$

This procedure is repeated every time the particle enters and leaves the zone of interest. For a typical CARPT run of 16 h the particle enters and leaves the bottom most zone ($Z = 0$–2 cm) more than 20,000 times and each of those visits contributes to the STD curve. The above procedure is repeated for all the other zones. All STDs are then calculated. In addition, the STD, like any other probability density function, can be characterized in terms of its moments like the mean value, standard deviation, skewness and kurtosis and this is also done. The definition of each of these statistical quantities is reviewed below.

The mean of the STD in the ith zone is denoted by μ_i and is defined by

$$\mu_i = \sum_{j=1}^{N_{\mathrm{tot}}} t_{\mathrm{resj}_i} E_i(t_{\mathrm{resj}})\Delta t. \tag{2}$$

Here N_{tot} corresponds to the number of particle occurences in zone i (20,000 for the bottom zone), t_{resj_i} is the sojourn time of the tracer particle during the jth trip to zone i of interest, as given by (1) and $E_i(t_{\mathrm{resj}})$ is the probability density function (p.d.f.) of the STD for that zone. The first moment (μ_i) provides an insight as to whether the region experiences low or high through flow. A region where the mean residence times are higher can

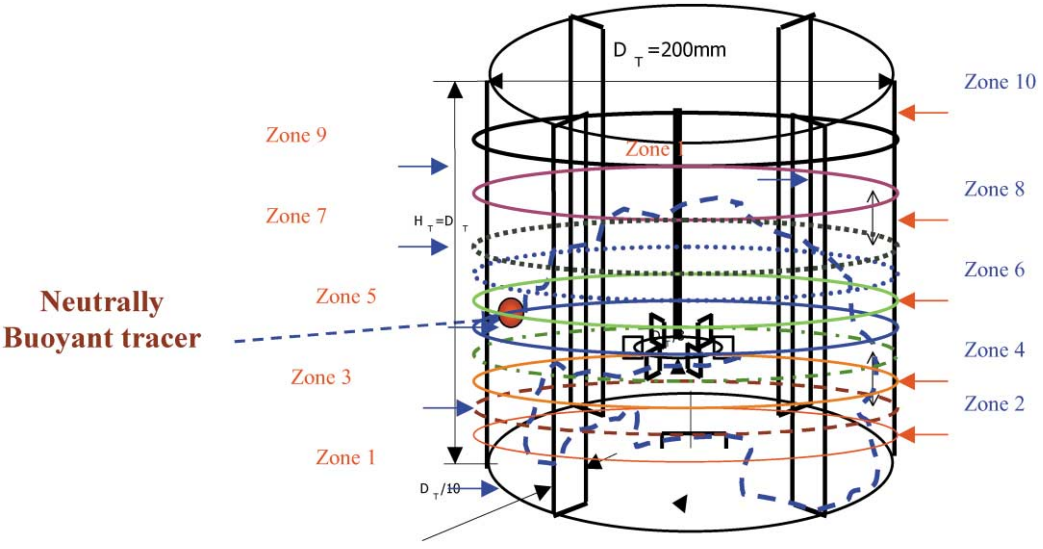

Fig. 10. Compartmentalization of the stirred tank into axial zones.

be thought of as a region of lower velocities and ultimately as dead zones.

The variance of the STD in the ith zone is denoted by σ_i^2 and is defined by

$$\sigma_i^2 = \sum_{j=1}^{N_{\text{tot}}} (t_{\text{resj}_i} - \mu_i)^2 E_i(t_{\text{resj}})\,\Delta t. \tag{3}$$

The positive square root of the variance is the standard deviation denoted by σ_i. σ_i^2 is also referred to as the second moment about the mean value and it indicates how "spread out" the STD is.

Skewness is the third moment about the mean, and is defined for the STD of the ith zone as

$$\gamma_{1_i} = \sum_{j=1}^{N_{\text{tot}}} \left(\frac{t_{\text{resj}_i} - \mu_i}{\sigma_i}\right)^3 E_i(t_{\text{resj}})\,\Delta t. \tag{4}$$

It is a measure of asymmetry of the distribution. If $\gamma_{1i} > 0$, the distribution is said to be skewed to the right and if $\gamma_{1i} < 0$, the distribution is said to be skewed to the left. If the p.d.f. of the variable is symmetric about the mean then $\gamma_{1i} = 0$.

The fourth moment about the mean is called kurtosis, and is defined for the STD of the ith zone as

$$\gamma_{2_i} = \sum_{j=1}^{N_{\text{tot}}} \left(\frac{t_{\text{resj}_i} - \mu_i}{\sigma_i}\right)^4 E_i(t_{\text{resj}})\,\Delta t - 3. \tag{5}$$

It reflects the degree to which the population is distributed in the tail of the distribution. $\gamma_{2i} > 0$ means that the data is concentrated around the mean (it is leptokurtic); $\gamma_{2i} < 0$ means that the data is concentrated in the tails of the distribution (it is platykuritic).

The CARPT data in the stirred tank have been processed as discussed above to generate the STD curves shown in Fig. 11. Inspection of the STDs in various zones

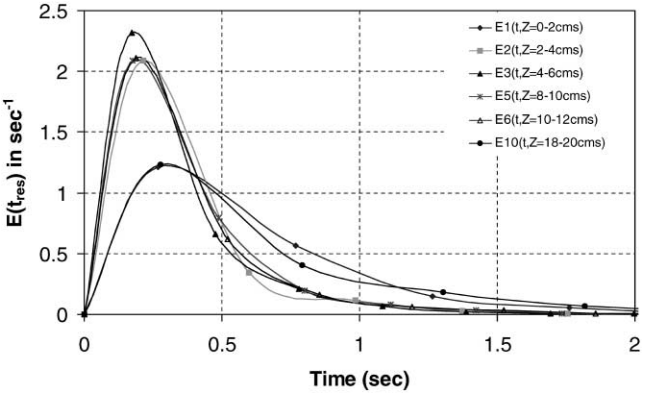

Fig. 11. Probability density functions of the sojourn time distributions in different axial zones of the STR from CARPT data.

reveals that there is a definite similarity in the shape of the STDs in the zones above (e.g., E_5 and E_6, etc.) and below the impeller (e.g., E_2 and E_3). It is also evident from Fig. 11 that the STD in the very bottom region (E_1) is very similar to that in the top most region (E_{10}). Moreover, the mean residence times and the standard deviations (variances) are the largest in these zones as shown in Fig. 12. As discussed earlier, flow visualization with polystyrene particles revealed stagnant zones in the bottom zones which were confirmed by CARPT. CARPT data interpreted in terms of STDs and their moments reveal that the stagnant zones can then also be expected in the top region in the tank where the standard deviation of the STD is even somewhat higher than in the zone at the bottom of the tank (see Fig. 12). Further compartmentalization of the tank for CARPT data processing can identify the precise location of such dead zones. Clearly, compartmentalization in the θ and r

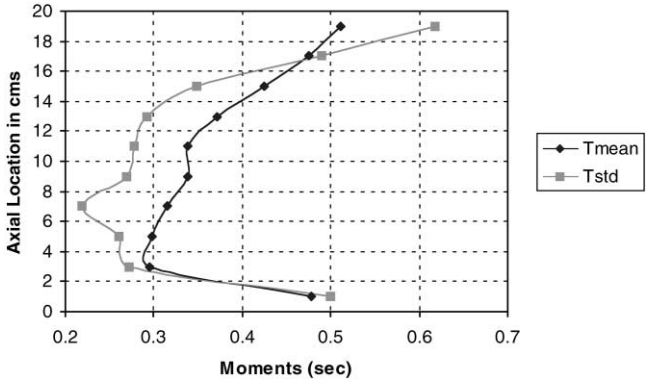

Fig. 12. Axial variation of the mean and of the standard deviation of the STDs.

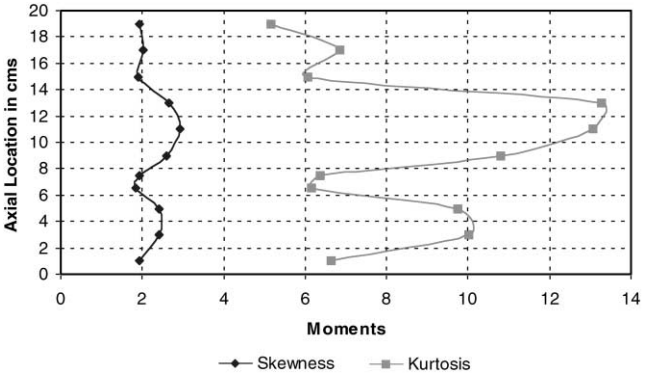

Fig. 13. Axial variation of the skewness and the kurtosis of the STDs.

Table 3
Different moments of the STD curves in various axial zones in a batch stirred tank

Zone	Z (cm)	T_{mean} (s)	T_{STD} (s)	Skewness	Kurtosis
1	0–2	0.4777	0.4999	1.9428	6.6237
2	2–4	0.2946	0.2727	2.4113	10.0190
3	4–6	0.2978	0.2599	2.4038	9.7555
4	6–8	0.3146	0.2190	1.30433	3.9123
5	8–10	0.3381	0.2693	2.6062	10.8040
6	10–12	0.3389	0.2780	2.9137	13.0560
7	12–14	0.3714	0.2918	2.6403	13.2760
8	14–16	0.4255	0.3490	1.8961	6.0530
9	16–18	0.4758	0.4894	2.0202	6.8590
10	18–20	0.5113	0.6182	1.9364	5.1530

directions would allow examination of the regions around the baffles, etc.

From the STD curves the different moments were extracted as per Eqs. (2)–(5) and are summarized in Table 3.

In Fig. 12, the axial variation of the mean and the standard deviation of the STD curves for the axially distributed compartements are shown. This figure indicates that the mean residence time is the highest at the top and the bottom of the tank which was also evident from Fig. 11. This trend is as expected since both at the top and the bottom of the tank the velocities are very low and, hence, once the particle enters these regions it tends to remain longer in these regions than in the impeller plane where the velocities are the highest. The mean residence time reaches a minimum in zone 2 ($Z = 2$–4 cm) and then increases progressively until it reaches its maximum value in the topmost zone. The axial variation of the standard deviation of the sojourn times reaches a minimum in the zone containing the impeller (Zone 4) and then increases exhibiting the same trend as the mean sojourn times. The lowest standard deviation in the impeller plane would seem to suggest that the flow in this region is the closest to plug flow with the deviation from plug flow increasing as we move away from this zone. This confirms the presence of an almost unidirectional radial jet in the impeller zone and regions of lower velocity near the bottom and top of the tank. The axial variation of the third and the fourth moments of the STDs are shown in Fig. 13. The skewness (third moment) is seen to be greater than zero in the entire tank which indicates that the distribution is skewed to the right throughout the tank. This skewness to the right is seen to be the smallest in the zone containing the impeller and at the bottom and the top portion of the tank. The kurtosis in the entire tank is greater than zero which suggests that the sojourn times are concentrated around the mean (i.e., it is leptokurtic) as evident from Fig. 11.

It should be reemphasized that we have compartmentalized the stirred tank into equal segments in the axial direction without partitioning in radial or azimuthal direction only as a matter of convenience and to illustrate the STD concept and demonstrate how CARPT data can be used to obtain STDs. The stirred tank could readily be divided into a two- or three-dimensional compartmental sections as demonstrated by Mann and coworkers (Mann, Williams, Dyakowski, Dickin, & Edwards, 1997) and CARPT data can be used to provide STDs of such compartments and to provide "connectiveness", i.e., flow exchange parameters between the compartments which are needed for mixer and reactor performance calculations.

In addition, various quantities for comparison with computational fluid dynamic codes (CFD) predictions can be evaluated from CARPT data.

4. Summary and conclusions

In this work, CARPT has been introduced as a technique for measuring the flow field in a stirred tank with single-phase flow. The striking feature of CARPT is that upon calibration, data that take months to collect with conventional laser-based techniques can be obtained in 16–20 h! It has been shown that the CARPT technique

can qualitatively capture many of the important flow structures observed in stirred tanks. The full three-dimensional Lagrangian measurements obtained by CARPT also provide both better flow visualization and quantitative measures of the specific features of the flow pattern, like the location of the eye of the recirculating loops and the shapes of the dead zones at the bottom of the tank. CARPT allows direct assessment of the sojourn time distributions in different parts of the stirred tank. A partial quantification of the dead and active zones was achieved by examining the obtained STD curves. A more detailed quantitative comparison of the mean velocity and turbulent velocity profiles obtained in different regions of the tank by CARPT to the values reported by conventional LDA and DPIV techniques is currently in progress. Such comparison will enable us to ascertain the limitations and the accuracy of the CARPT measurements in single-phase flows before we embark on multiphase flow studies in stirred tanks.

Notation

D, T, D_T	tank diameter, cm
D_i	impeller diameter, cm
H_T	height of liquid in tank, cm
N	rpm
r, R	radial distance, cm
V_r	mean radial velocity, cm/s
V_θ	mean tangential velocity, cm/s
V_z	mean axial velocity, cm/s
Z	axial distance
Re	Reynolds number
t	time, s

Greek letters

γ_1	third moment of the STD
γ_2	fourth moment of the STD
Δ	incremental change
μ	first moment of the STD
σ^2	second moment of the STD

Acknowledgements

The authors would like to thank the sponsors of the Chemical Reaction Engineering Laboratory (CREL) for making this research possible.

References

Costes, J., & Couderc, J. P. (1988a). Study by LDA of the turbulent flow induced by a Rushton turbine flow induced by a Rushton turbine in a stirred tank influence of the size of the units — I. Mean flow and turbulence. *Chemical Engineering Science*, *43*(10), 2751–2764.

Costes, J., & Couderc, J. P. (1988b). Study by LDA of the turbulent flow induced by a Rushton turbine flow induced by a Rushton turbine in a stirred tank influence of the size of the units—II. Spectral analysis and scales of turbulence. *Chemical Engineering Science*, *43*(10), 2765–2772.

Chaouki, J., Larachi, F., & Dudukovic, M. P. (1997). *Non-invasive monitoring of flows* (p. 48). Amsterdam, The Netherlands: Elsevier (Chapter 2).

Deen, N. G., & Hjertager, B. H. (1999). *Multiphase particle image velocimetry measurements in an aerated stirred tank*. Paper prepared for presentation at the 1999 Annual Meeting of A.I.Ch.E., Dallas, Tx, Oct 31–Nov 5, Session 06005: Solid–Liquid & Gas–Liquid Mixing, Unpublished.

Degaleesan, S. (1997). *Fluid dynamic measurements and modeling of liquid mixing in bubble columns*. D.Sc. thesis, Washington University, St.Louis, MO.

Degaleesan, S., & Dudukovic, M. P. (1995). *Measurement of turbulent dispersion coefficients in bubble columns using CARPT*. Mixing X, Banff, Canada, June.

Devanathan, N. (1991). *Investigation of liquid hydrodynamics in bubble columns via Computer Automated Radioactive Particle Tracking (CARPT)*. D.Sc. thesis, Washington University, St.Louis, MO.

Devanathan, N., Moslemian, D., & Dudukovic, M. P. (1990). Flow mapping in bubble columns using CARPT. *Chemical Engineering Science*, *45*(8), 2285–2291.

Gunkel, A. A., & Weber, M. E. (1975). Flow phenomena in stirred tanks-I, Impeller-stream. *A.I.Ch.E. Journal*, *21*(5), 931–949.

Holland, F. A., & Chapman, F. S. (1966). *Liquid mixing & processing in stirred tanks* (pp. 11–14). New York: Reinhold publns.

Kemoun, A. (1995). *Experimental characterization of the structures in a stirred tank reactor*. Ph.D. thesis, Institut National polytechnique de Lorraine, Nancy, France.

Kemoun, A., Lusseyran, F., Mallet, J., & Mahoust, M. (1998). Experimental scanning for simplifying the model of a stirred tank flow. *Experiments in Fluids*, *25*, 23–36.

Kumar, S. B., & Dudukovic, M. P. (1997). Computer assisted gamma and X-ray tomography: Application to multiphase flow. In Chaouki, J., Larachi, F., & Dudukovic, M. P., (Eds.), *Non-invasive monitoring of multiphase flows*. Amsterdam, The Netherlands: Elsevier.

Larachi, F. G., Kennedy, G., & Chaouki, J. (1994). A gamma ray detection system for three dimensional Particle Tracking in Multiphase Reactors. *Nuclear Instruments and Methods in Physics Research*, *A338*, 568–576.

Mann, R., Williams, R. A., Dyakowski, T., Dickin, F. J., & Edwards, R. B. (1997). Development of mixing models using electrical resistance tomography. *Chemical Engineering Science*, *52*(13), 2073–2085.

Morud, K. E., & Hjertager, B. H. (1996). LDA measurements and CFD modeling of gas–liquid flow in a stirred vessel. *Chemical Engineering Science*, *51*(2), 233–249.

Ranade, V. V., & Joshi, J. B. (1990). Flow generated by a disc turbine. *Transactions of Institution of Chemical Engineers*, *68*(A), 19–50.

Rousar, I., & Van den Akker, H. E. A. (1994). LDA measurements of liquid velocities in sparged agitated turbines with single and multiple Rushton turbines. *Institution of Chemical Engineers Symposium Series*, *136*, 89–96.

Roy, S., Chen, J., Kumar, S. B., Al Dahhan, M. H., & Dudukovic, M. P. (1997). Tomographic and particle tracking studies in a liquid–solid riser. *Industrial and Engineering Chemistry Research*, *36*(11), 4666–4669.

Schaeffer, M., Hofken, M., & Durst, F. (1997). Detailed LDV measurements for visualization of the flow field within a stirred tank reactor equipped with a Rushton turbine. *Transactions of Institution of Chemical Engineers*, *75*(A), 729–736.

Schaefer, M., & Hofken, M. (1999). *Experimental study of trailing vortices around impeller blades*. Presented at Mixing XVII, August 15–20, Banff, Alberta, Canada.

Stoots, C. M., & Calabrese, R. V. (1995). Mean velocity field relative to a Rushton turbine blade. *A.I.Ch.E. Journal*, *41*(1), 1–11.

Tsoulfanidis, N. (1983). *Measurement and detection of radiation.*. New York: McGraw-Hill.

Van't Reit, K., & Smith, J. M. (1975). The trailing vortex system produced by Rushton turbine agitators. *Chemical Engineering Science*, *30*, 1093–1105.

Van der Molen, K., & van Maanen, H. R. E. (1978). Laser Doppler measurements of the turbulence flow in stirred vessels to establish scaling rules. *Chemical Engineering Science*, *33*, 1161–1168.

Wu, H., & Patterson, G. K. (1989). LDA measurements of turbulent flow parameters in a stirred mixer. *Chemical Engineering Science*, *44*(10), 2207–2221.

Wittmer, S., Falk, L., Pitiot, P., & Vivier, A. (1998). Characterization of Stirred vessel hydrodynamics by three dimensional trajectography. *Canadian Journal of Chemical Engineering*, *A7*(6), 600–610.

Yianneskis, M., Popilek, Z., & Whitelaw, J. H. (1987). Steady and unsteady flow characteristics of stirred reactors. *Journal of Fluid Mechanics*, *175*, 537–555.

Yianneskis, M., & Whitelaw, J. H. (1993). On the structure of the trailing vortices around Rushton turbine blades. *Transactions of Institution of Chemical Engineers*, *71*(A), 543–550.

Zhou, G., & Kresta, S. M. (1996). Distribution of energy between convective and turbulent flow for three frequently used impellers. *Transactions of Institution of Chemical Engineers*, *74*(A), 379–389.